energies

MDPI

Article

Spotted Hyena Optimization Method for Harvesting Maximum PV Power under Uniform and Partial-Shade Conditions

Ezhilmaran Ranganathan and Rajasekar Natarajan *

Solar Energy Research Cell (SERC), School of Electrical Engineering, Vellore Institute of Technology, Vellore 632014, Tamilnadu, India; ezhilmaran.r2015@vit.ac.in

* Correspondence: nrajasekar@vit.ac.in; Tel.: +91-9952362301

Abstract: Maximum power-point-tracking techniques applied for partially shaded photovoltaic array yield maximum power output via operating the panel at its most efficient voltage. Considering the noticeable issues existing with the available methods, including steady-state oscillations, poor tracking capability and complex procedures, a new bioinspired Spotted-Hyena Optimizer (SHO) is proposed. It follows simple implementation steps, and does not require additional controller-parameter tuning to track the optimal power point. To validate the versatility of the proposed method, the SHO algorithm is applied to track the maximum power of different string arrangements under six partial-shade conditions. Further, to authenticate SHO's methods, its results are compared with perturb-and-observe (P&O), and particle-swarm-optimization (PSO) methods. As a result of its implementation, it is observed that the tracking speed of SHO towards the global convergence for four patterns under 4S2P are 0.34 s, 0.24 s, 0.2 s, and 0.3 s, which is far less than the PSO and P&O methods. Further, to demonstrate its suitability, a hardware prototype is built and tested for various operating conditions. The experimental results are in good agreement with the simulated values.

Keywords: maximum power point tracking (MPPT); optimization; partial shading; perturb-and-observe algorithm (P&O); photovoltaic (PV) array; solar energy

Citation: Ranganathan, E.; Natarajan, R. Spotted Hyena Optimization Method for Harvesting Maximum PV Power under Uniform and Partial-Shade Conditions. *Energies* **2022**, *15*, 2850. https://doi.org/10.3390/en15082850

Academic Editors: Antonio D'angola and Alessandro Ciocia

Received: 13 February 2022
Accepted: 21 March 2022
Published: 13 April 2022

1. Introduction

With numerous benefits such as zero noise, zero pollution, and less maintenance, power generation from PV installations has increased up to 49% globally in the last decade [1]. Whilst being employed in many sectors, the main frailty associated with PV modules are limited conversion efficiency, high capital investment, and hindrance in output power due to partial shading (PS). Accumulation of dust, bird spitting, soiled panels due to aging, and passage of clouds are its major causes [2–4]. Hence, to handle PS and improve energy yield, many maximum power-point-tracking (MPPT) techniques are proposed. Some of desirable characteristics of MPPT are high tracking accuracy, faster convergence, ability to eliminate local peaks, and lesser oscillations. Thus, the tracking of maximum power points (MPP) has been the subject of study for the past few decades. Various MPPT methods seen in literature can be categorized into (1) analytical and (2) bioinspired methods.

The well-recognized analytical MPPT methods such as fractional short-circuit current [5], hill-climbing (HC) algorithm [6], incremental conductance (Inc. Cond.) [7], perturb and observe (P&O) [8], and fractional open-circuit voltage [9] often show incredible characteristics such as less complexity, easy implementation, and good tracking performance at zero shade. However, the majority of them are prone to steady-state oscillations, tracking efficiency subject to duty-cycle initialization, and ineffectiveness during PS conditions.

Thus, fuzzy logic control (FLC) [10] and artificial neural network (ANN) [11] are used as alternative methods. However, as an alternative method, the requirement of period training, involvement of large memory to handle a voluminous dataset, and high computational burden restricts its usage.

Other than the above, optimization techniques with the ability to solve nonlinear multi-model optimization problems effectively are also often used for MPPT. These techniques are extremely popular due to their quick response, faster convergence to MPP even in PS condition, and high efficiency at any shade conditions [12]. Different optimization techniques attempted so far include teaching learning-based optimization (TLBO) algorithms [13], the fireworks algorithm [14], wind-driven optimization (WDO) [15], salp-swarm optimization (SSO) [16,17], moth-flame optimization (MFO) [18], grey-wolf optimization (GWO) [19], cuckoo-search optimization [20], tunicate-swarm optimizer [21], squirrel search [22], and musical chairs algorithms [23].

Most often, particle-swarm optimization (PSO) [24] and its variants such as modified PSO [25,26], velocity-based PSO [27], and levy-flight PSO [28] are employed for power tracking. However, the system performance is tampered due to premature convergence and poor balance between exploration and exploitation. To resolve such limitations, nested loops in PSO [29] and fast adaptive PSO [30] are introduced. Nevertheless, to achieve enhanced solutions, the merits of two methods are hybridized. For instance, PSO with P&O [31], PSO and shuffled frog-leaping algorithm (SFLA) [32], grey-wolf optimizer alongside with fuzzy logic control (GWO-FLC) [33], and fireworks combined with P&O [34], ANN combined with INC (ANN-INC) [35], and Gaussian process regression with Jaya algorithm (GPR-Jaya) [29] are made to enhance convergence. Although hybridization is incorporated in PSO, GWO methods show improvements in performance at the cost of large computation time [31,33], even though sometimes the strengths of these techniques have been ignored. Moreover, additional parameter tuning increases complexity and prolongs settling time [36].

Hence, exploring new methods for MPPT and detailing about its merits in achieving best results is inevitable. Therefore, with the objective of accurately tracking the global peak in the presence of partial-shading conditions, a new method utilizing the behavior of Spotted Hyena is proposed. This stochastic optimization technique proves to be superior in solving complex numerical and nonlinear computational problems effectively [31]. Further, the notable characteristics of the SHO method are a good balance among population-based searches during exploration (the process of searching in a bigger area of search space for promising solutions) and exploitation (restricting the search to a small area of the search space), fewer tuning parameters, and easy implementation. Thus, based on its distinctive characteristics it is expected to produce minimal power fluctuations and faster convergence with low steady-state oscillations [31].

The proposed technique's performance is assessed in both simulation and hardware to verify its effectiveness. Various experiments have been carried out with various shade patterns on PV arrays/strings of various sizes. Furthermore, a detailed analysis is performed using the SHO simulated findings as well as well-established methodologies such as P&O and PSO. Furthermore, the superiority of these techniques has been demonstrated in a variety of pattern-change scenarios. The SHO method's capabilities in terms of global MPP convergence at minimal settling time and zero steady-state oscillations is supported by performance analysis and experimental testing.

This paper is organized in subsequent sections, detailed as follows: Section 2 deals with SPV modeling and describing the impacts of PS conditions. Further, Section 3 briefly presents the SHO algorithm, and Section 4 explains the obtained simulation and experimental results with the proposed SHO method and its comparative study with P&O and PSO. Moreover, the obtained results are also compared with existing literature to prove the efficacy of SHO methods.

2. Modeling of PV Module

Typically, a solar PV cell can be represented by an electrical equivalent circuit model that comprises of an ideal current source, diode, and resistors. Because of the nonlinearity characteristics, several modeling methods evolved in the recent past to model PV characteristics. Prominently used PV models are one-diode, two-diode, and three-diode models. The

number of diodes present indicates the accuracy of V-I curves predicted with additional implementation complexity.

2.1. Single-Diode Model

Due to simplicity, the single-diode model of the PV module is commonly used in practice for modeling and simulation purposes. It is found that in many cases, the accuracy of the single-diode PV model is satisfactory, even after neglecting diode-recombination losses [33,34]. The photovoltaic cell modeling using a single-diode electrical equivalent circuit is depicted in Figure 1. The series resistor (R_s) and parallel resistance (R_{sh}) account for metallic junction loss and recombination loss that occur in a diode, respectively.

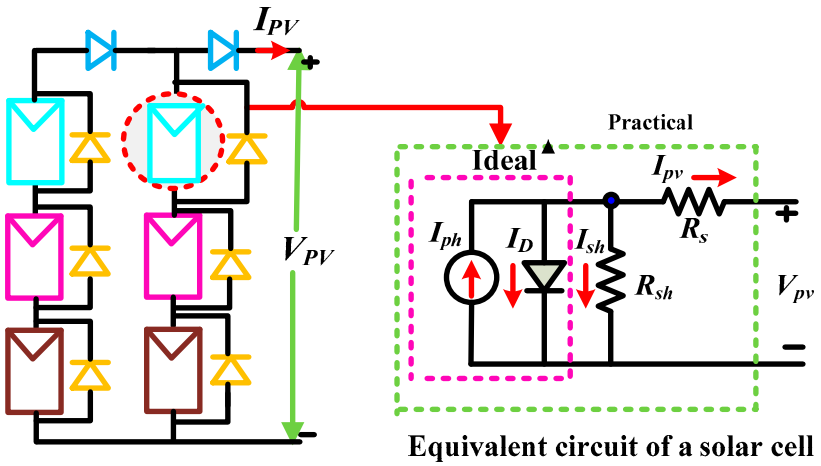

Figure 1. Equivalent circuit representation of single-diode model.

Applying KCL, the output current of the solar PV cell is obtained using

$$I = I_{PV} - I_D - \frac{V + IR_S}{R_P} \tag{1}$$

Assuming the diode to be ideal, its corresponding diode current I_D equation is given by

$$I_D = I_0(e^{\frac{V_D}{aV_t}} - 1) \tag{2}$$

where a is the diode ideality factor and its thermal voltage V_t is defined for any value of temperature T (Kelvin) in the below equation:

$$V_t = N_s kT/q \tag{3}$$

where q is the electron charge equal to 1.6×10^{-19} C, k is the Boltzmann constant equal to 1.3805×10^{-23} J/K and N_s is the number of series-connected cells forming the PV module.

2.2. Impact of Partial Shading and Significance of MPPT

PV modules when arranged in series and parallel form a PV string or array. A PV string is formed by connecting modules in series (6S); while strings are in parallel, they form a PV array (6S2P). The relevant PV characteristics of both unshaded and shaded array are depicted in Figure 2.

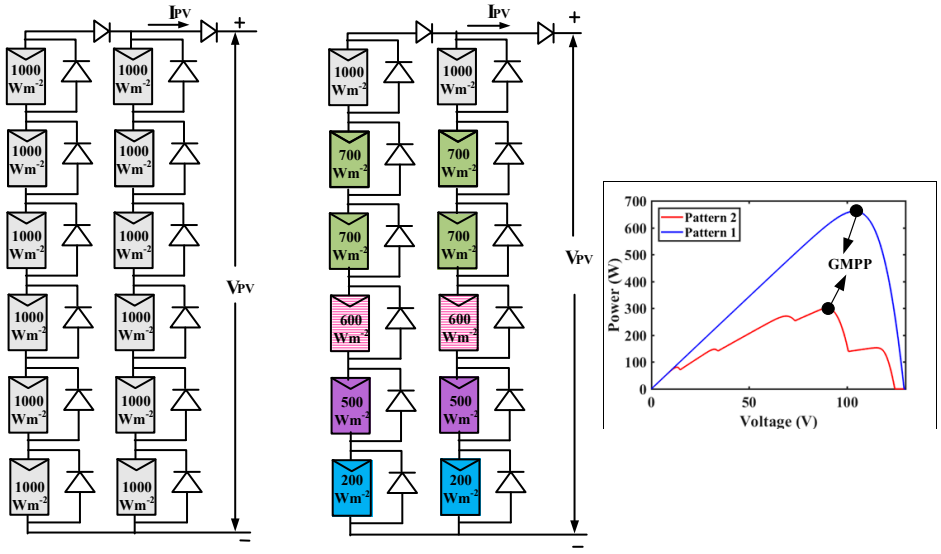

Figure 2. Occurrence of single and multiple power peaks during uniform and partial shade conditions.

Here, it is noteworthy to mention that the PV characteristics vary depending on the irradiance and temperature that the module receives. For instance, PV array with zero shade i.e., uniform irradiance at 100 W/m^2 and at a temperature of 25 °C, produces a single power peak. Meanwhile, panels with shade introduce multiple peaks, causing voltage differences due to shade activating the bypass diode; hence, panels are effectively bypassed for safety.

MPP tracking is used in power electronic converters to electronically extract the maximum power delivered by PV string/array to handle the effect of partial shade. Various MPPT algorithms are expected to be proposed in order to achieve maximum power. The effectiveness of tracking, on the other hand, is determined by the procedure employed. PS causes both local and global MPP when it occurs. As a result, caution must be exercised when developing the MPPT approach. Many bioinspired strategies have recently evolved to achieve a better solution to the given optimization challenge.

A new technique based on the hunting behavior of Spotted Hyena is proposed in this work. The major advantage associated with the method includes faster convergence, avoidance of local power settlement, no controlling-parameter tuning, and optimum convergence time.

3. Spotted-Hyena Optimizer

The Spotted-Hyena Optimizer (SHO) is a swarm-based metaheuristic optimization algorithm that solves constrained and unconstrained optimization problems using a hierarchy based on social and hunting behavior within a clan of spotted hyenas. The close-knit clusters help the spotted hyena clan members work together in a well-ordered manner to improve hunting effectiveness. Observation, gleaning, and scent are used by spotted hyenas to track for possible prey. Trailing, chasing, encircling, and ambushing mechanisms are shown in Figure 3 as different phases of spotted-hyena hunting behavior. The first step is prey tracking, in which possible prey targets are scouted from the entire roster; the second phase is prey chasing and rundown, in which prey is carefully isolated from the group to reduce disruption throughout the overall hunting process. The encircling and harassing phase is the third phase, during which the numerous members of the spotted hyena clan disperse the hunt's spoils in a methodical and hierarchical order of precedence.

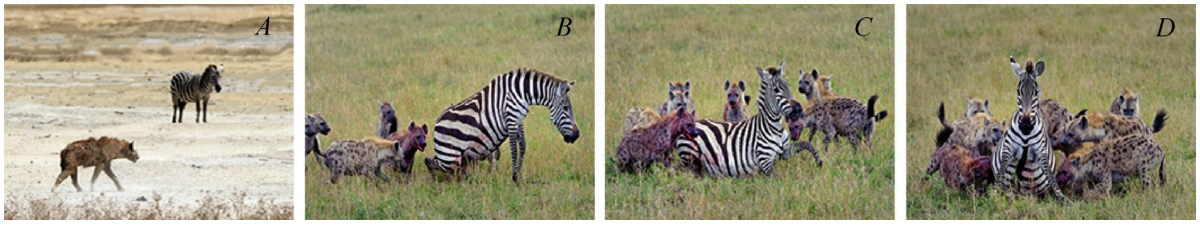

Figure 3. Various phases of spotted hyena hunting behavior: (**A**) searching and tracking prey; (**B**) chasing; (**C**) troublesome and encircling; (**D**) immobilize situation and attack prey [31].

Spotted hyenas hunt their prey in packs or clusters; these cooperative clan animals scout and attack prey in a well-coordinated manner. Every hyena updates its position with regard to the prey position, since the latter represents the solution to a given optimization problem. Moreover, hyenas in the cluster update their distance with respect to the prey; therefore, it must be reduced before attacking the prey. Since the prey position is initially unknown, the best position of the targeted prey and other hyena locations are updated. This behavior is mathematically modeled as

$$\vec{D_h} = \left| \vec{B} \cdot \vec{P_p}(x) - \vec{P}(x) \right| \tag{4}$$

$$\vec{P}(x+1) = \vec{P_p}(x) - \vec{E} \cdot \vec{D_h} \tag{5}$$

In the above equation to promote exploration as well as randomness to avoid the convergence to local optima, SHO uses vectors B and E as coefficients. Further, P_p, P and D_h represent the best, current positions of the hyena and the distance between spotted hyena and prey, respectively. These vectors are computed using:

$$\vec{B} = 2 \cdot \vec{rd_1} \tag{6}$$

$$\vec{E} = 2\vec{h} \cdot \vec{rd_2} - \vec{h} \tag{7}$$

$$h = 5 - \frac{(iteration * 5)}{Max\_iterations} \tag{8}$$

To have an equilibrium between exploration and exploitation, the value of the 'h' vector is linearly reduced from 5 to 0 until maximum iteration is reached. Here, the random vectors rd_1 and rd_2 take values in [0, 1]; application of Equations (4) and (5) in two-dimensional form is indicated in Figure 4. In this figure, the spotted hyena (A,B) can update its position towards the position of prey ($A*$, $B*$).

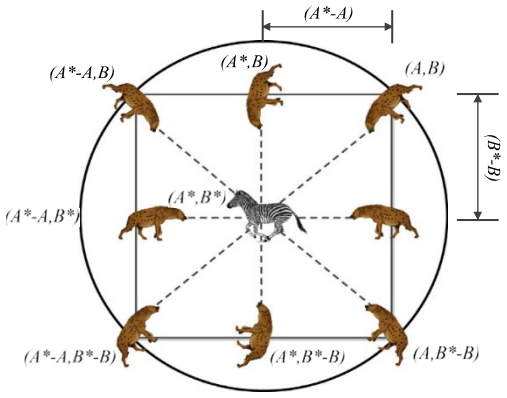

Figure 4. Two dimensional position of spotted hyena.

The number of optimal positions in the group or cluster during the hunting phase is recorded based on the coefficient vector E and is given by

$$C_h = P_k + P_{k+1} + \ldots . P_{k+N} \tag{9}$$

where P_k indicates the accompanying location of spotted hyenas and P_h is defined as foremost best spotted hyena location. Here, N indicates the number of spotted hyenas which is enumerated as follows:

$$N = count_{nos}(P_h + P_{h+1} + \ldots .(P_h + M)) \tag{10}$$

where M is a vector which is random between the range of [0.5, 1] and C_k is a cluster or group of N optimal solution numbers. Hyenas attack the prey when they are in close proximity to the prey; this is indicated mathematically using the coefficient vector E. When the vector $E < 1$, the pack of spotted hyenas moves in to kill the prey. The attacking of prey is mathematically represented as follows:

$$P(x+1) = \frac{C_h}{N} \tag{11}$$

where $P(x+1)$ captures the preeminent solution and location updates of the other search entities in accordance with the position of the preeminent entity of search. The final termination of the SHO algorithm is conducted through the satisfaction of a termination criterion. The hunt and attack of the prey are pictorially presented in Figures 5 and 6, respectively. The complete algorithm steps are indicated with the help of the flowchart in Figure 7.

Figure 5. Searching for prey ($|E| > 1$).

Figure 6. Attacking prey ($|E| < 1$).

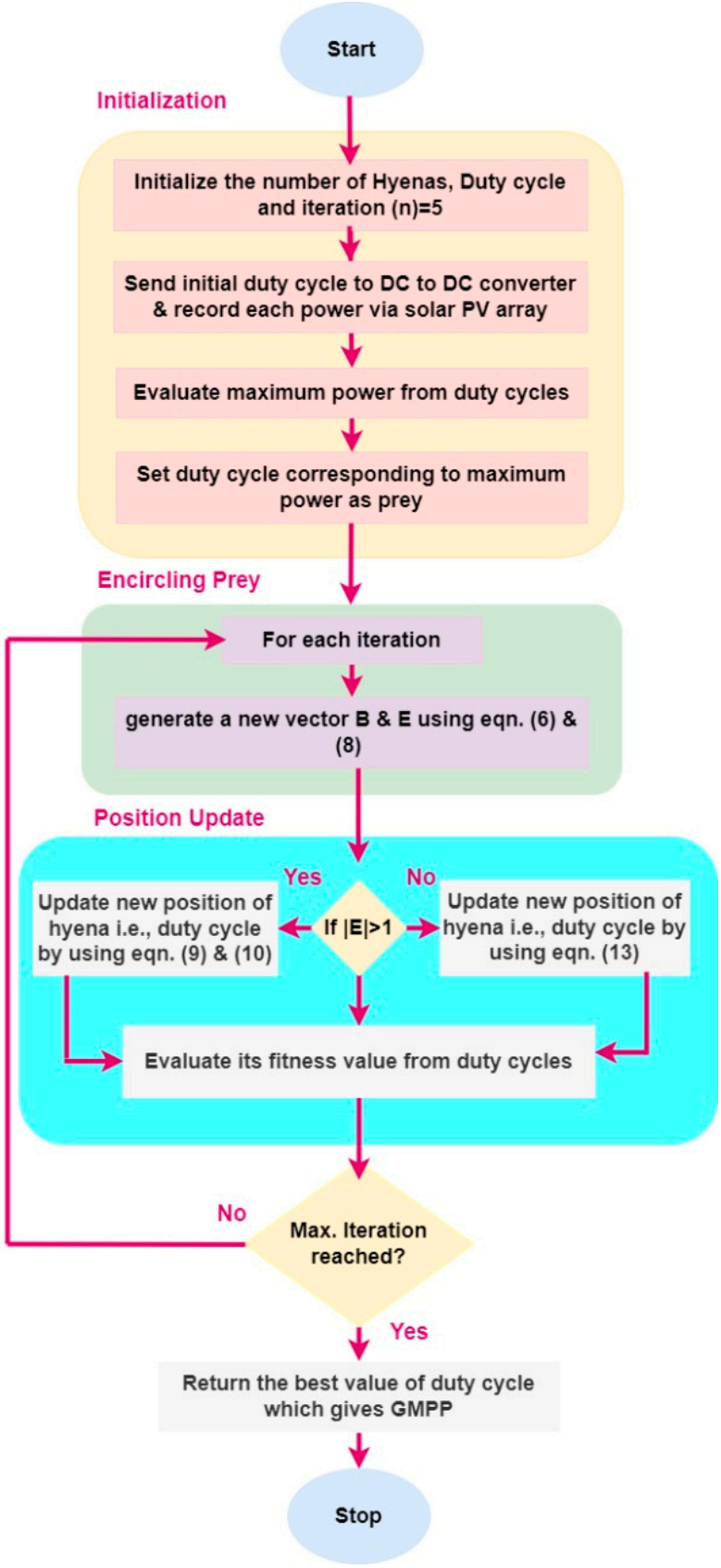

Figure 7. Flow chart for SHO.

4. Results and Discussions

Simulations are run for three distinct PV array designs with six different shade patterns, encompassing both uniform and partial-shade circumstances, with the goal of testing the efficacy of the suggested SHO approach. As a result, specific software codes for SHO, P&O, and PSO algorithms have been written in MATLAB for simulation. The software application for all three methods is built and tested for the PV array configuration shown in Figure 8. A DC–DC converter and a digital MPPT controller with inputs from voltage and current sensors make up the system setup.

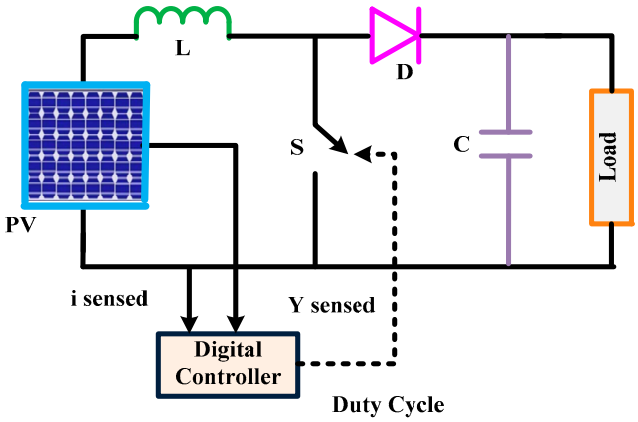

Figure 8. Block diagram of simulated system.

The MPPT controller is used to implement all of the MPPT techniques. The parameter values C and L of a DC–DC boost converter are 330F and 10 mH, respectively, and this is meant to run in continuous mode. The switch operates at a 10 kHz frequency. For algorithm testing, an additional R load of 50 volts is supplied to the converter. Under identical test conditions, existing methodologies such as P&O and PSO methods are also used for comparison. The values are obtained from the current literature to reach the best feasible answer because the settling point of the PSO method is dependent on the suitable selection of controlling parameters.

Further, the simulation-sampling period is chosen as 0.03 s. As previously mentioned, three types of PV arrangements with 4 × 2, 5 × 1, and 6 × 1 panels are used. Various uniform and partial-shade conditions that have been utilized for testing are indicated in Figure 9. As indicated in Figure 9–Pattern 1, uniform irradiation, i.e., zero shade, refers to the standard test condition (STC) of 1000 W/m^2 at 25 °C, while during partial-shade conditions, irradiation levels of PV modules are kept lower than STC at a constant temperature of 25 °C. Different shades applied for the 4 × 2, 5 × 1, and 6 × 1 PV arrays built are indicated in Figure 9–Pattern 2 to 6, respectively. While selecting the patterns for simulation, specific measures have been taken to diversify the occurrences of local and global peaks in order to test the method validity at different operating conditions. With each shade is given a unique pattern number—say, 1 to 6—its PV curves plotted for different test patterns indicate the occurrence of multiple local peaks due to panel bypass. During simulation, it is confirmed that all three techniques are compared and analyzed at the same instant and operating conditions in order to estimate the efficiency of the proposed algorithm under the same scenario. Further, the details of the panel specifications used are indicated in Table 1. The GMPP values for Patterns 1–6 are 439.8, 320.2, 206.8, 210, 105, and 120.2 W, respectively.

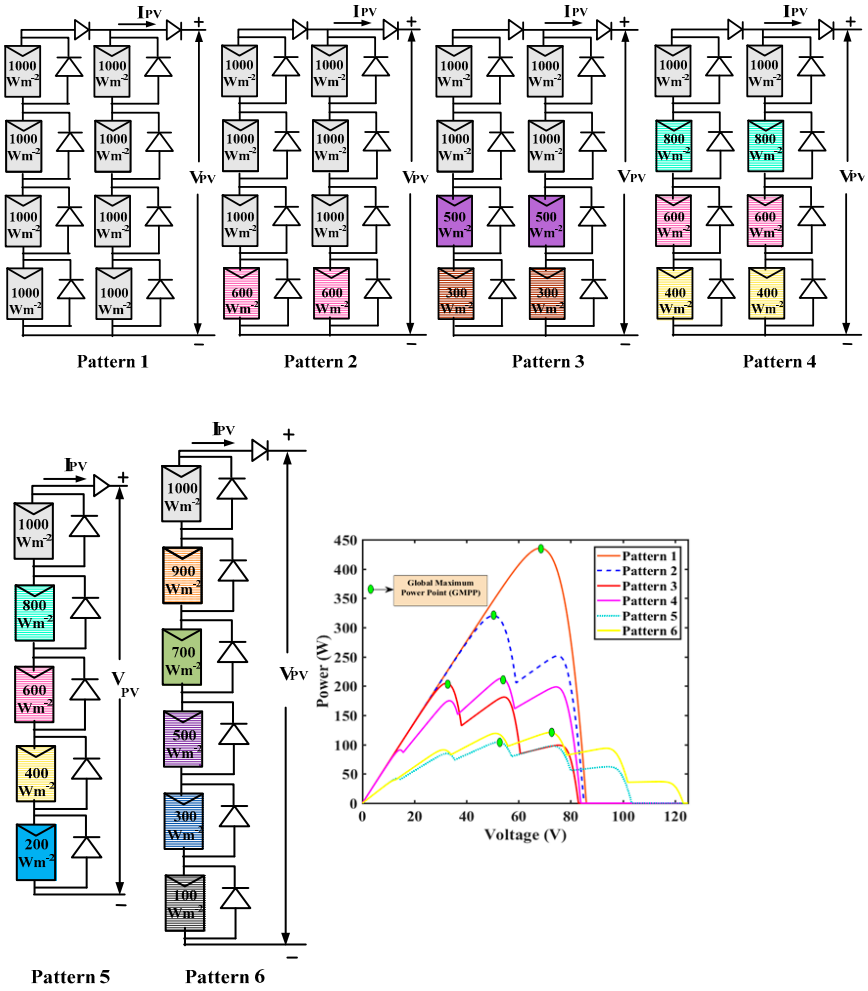

Figure 9. Various shade case of 4 × 2, 5 × 1, and 6 × 1 PV array along with its PV curve considered under study.

Table 1. Technical specification of simulated system.

S.No	Parameter	Value
1	Power rating	440 W
2	Inductor	10 mH
3	Capacitor	330 uF
4	Switching Frequency	10 kHz
S. No	**SM 55 PV Panel Details**	**Value**
1	Maximum PV Module Power (P_{mpp})	55 W
2	Maximum PV Module Voltage (V_{mpp})	17.4 V
3	Maximum PV Module Current (I_{mpp})	3.15 A
4	PV Module Open Circuit Voltage (V_{oc})	21.7 V
5	PV Module Short Circuit Current (I_{sc})	3.45 A

The system was tested with and without pattern change in two different scenarios. In Case A, throughout the simulation, just one pattern was used to determine the technique convergence features, speed of convergence, and capacity to detect the global peak. Case B, on the other hand, introduces pattern modifications inside the simulation time limit. This

discovery is crucial for understanding the method's behavior during abrupt transitions. The PV power, voltage, current, and duty cycle obtained in each simulation are recorded.

4.1. Case Study—A

4.1.1. Pattern 01 (MPPT under Zero or Uniform Shading)

In this pattern, all the panels of 4 × 2 PV array receive equal irradiance of 1000 W/m^2 at 25 °C. Under this condition, only a single power peak emerges at 439 W. Reaching the peak is not a laborious task for any method; however, this case is helpful to understand the time taken for convergence. As it is valid to point out that P&O method convergence depends upon initialization, the method converges to peak value at 1.35 s with initial duty of 0.5, while the PSO method reaches the peak at half of the P&O time at 0.78 s. On the other hand, SHO takes the lowest time relatively among the methods, at 0.34 s. The obtained simulation results are plotted in Figure 10. It can be inferred that during the search process both the SHO and PSO method experience variations in voltage, current, and power values due to random initial guess. Meanwhile, P&O follows a definite increment in duty value, hence no oscillations are observed at steady state. The performance of SHO is proved to be superior at uniform shading in comparison to the P&O and PSO techniques.

Case—A

Pattern 1

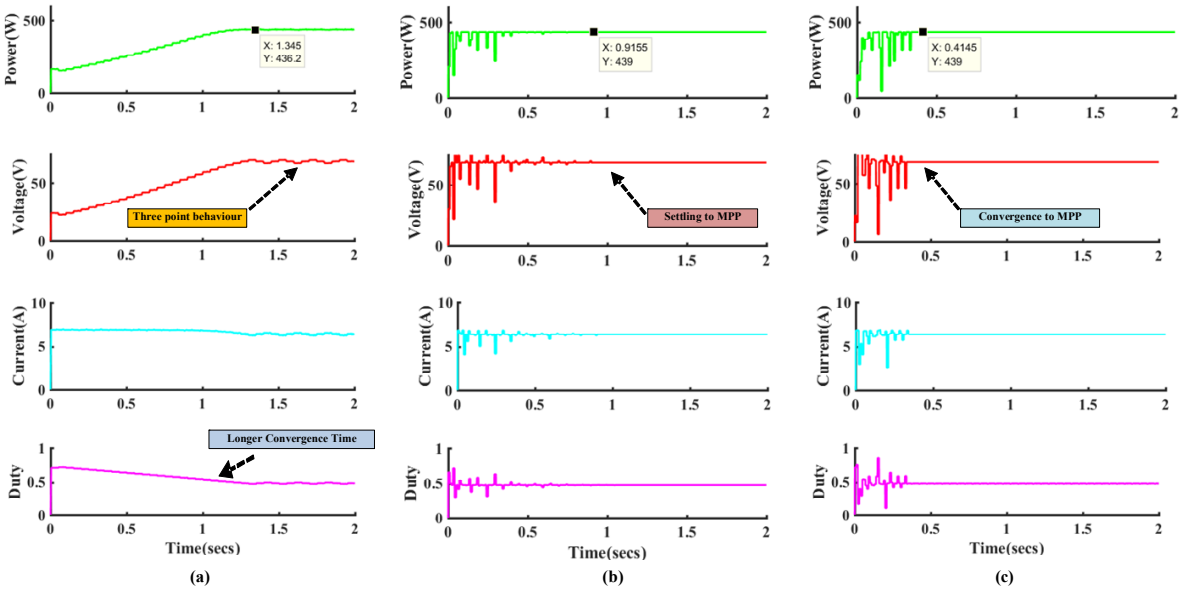

Figure 10. Simulated waveforms of (**a**) P&O, (**b**) PSO, and (**c**) SHO methods under Uniform irradiation (Pattern 1).

4.1.2. Pattern 02 (MPPT under Partial Shading—Two Peaks)

In this pattern, the last row of the 4 × 2 PV array is exposed to a shade of 600 W/m^2, creating two power peaks: (1) closer to V_{oc} of PV array, and (2) far from V_{oc}, as indicated in Figure 9. The details of the power peaks appearing in the PV curve are: 315 W global peak and 250 W local peak. The obtained simulation results are depicted in Figure 11. All the three methods managed well to converge at a global peak of 315 W. However, the P&O and PSO methods' convergences to a global peak of 315 W took 0.95 s and 1.23 s, respectively, while in the case of PSO there were larger oscillations as well as took large time for convergence. It is important to note that P&O is able to converge at a global peak under partial shading due to the initial duty-cycle initialization from the left side of the curve. At the same time, there will be higher probability that P&O will converge to the local power peak when it is incorrectly initiated. The better performance of SHO continues

in Pattern 2 as well, since the method had converged to a global peak of 315 W in 0.24 s with minimal oscillations.

Pattern 2

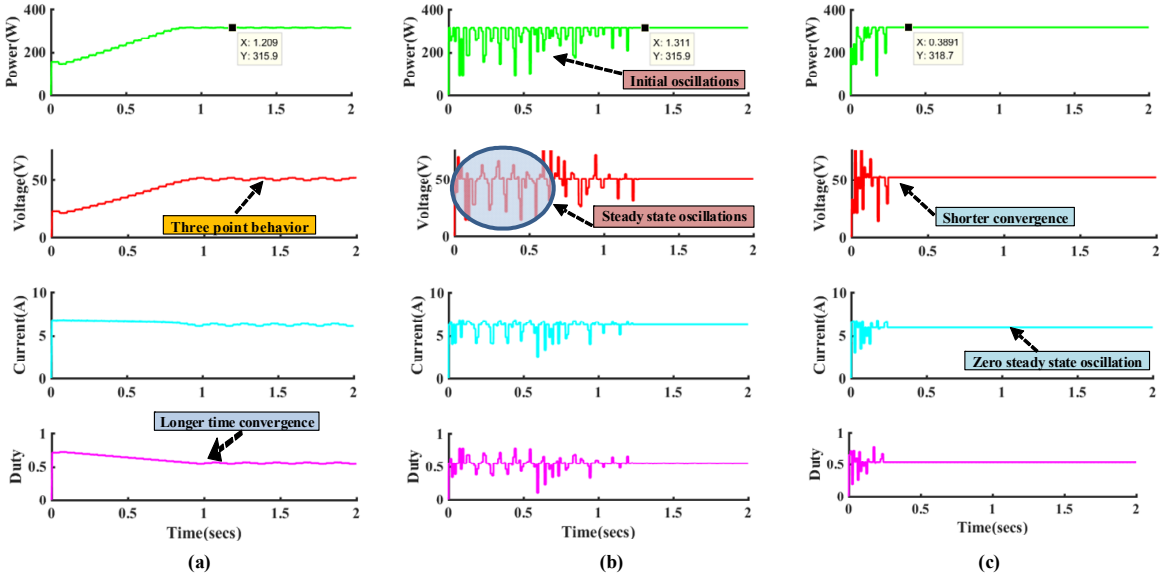

Figure 11. Simulated waveforms of (**a**) P&O, (**b**) PSO and (**c**) SHO methods for Pattern 2.

4.1.3. Pattern 03 (MPPT under Partial Shading—Three Peaks)

The earlier two patterns proved the assimilating performance of the SHO method, hence the additional local peak in close proximity with the global peak is created in Pattern 3. This case is important to estimate the capability of the SHO method to differentiate between the global and local peak and the amount of randomness created during the search process. The three power peaks include two local peaks of 175 W and 90 W and one global peak at 206.8 W, respectively. Referring to Figure 12, of the three methods the SHO method reaches a global peak of 203 W in 0.2 s, while PSO makes a larger oscillation to reach the global peak of 201.1 W. Above all, from the simulation result it is clear that the P&O and PSO methods converge nearer to the global peak of 201.1 W at 0.61 s and 1.4 s, respectively.

Pattern 3

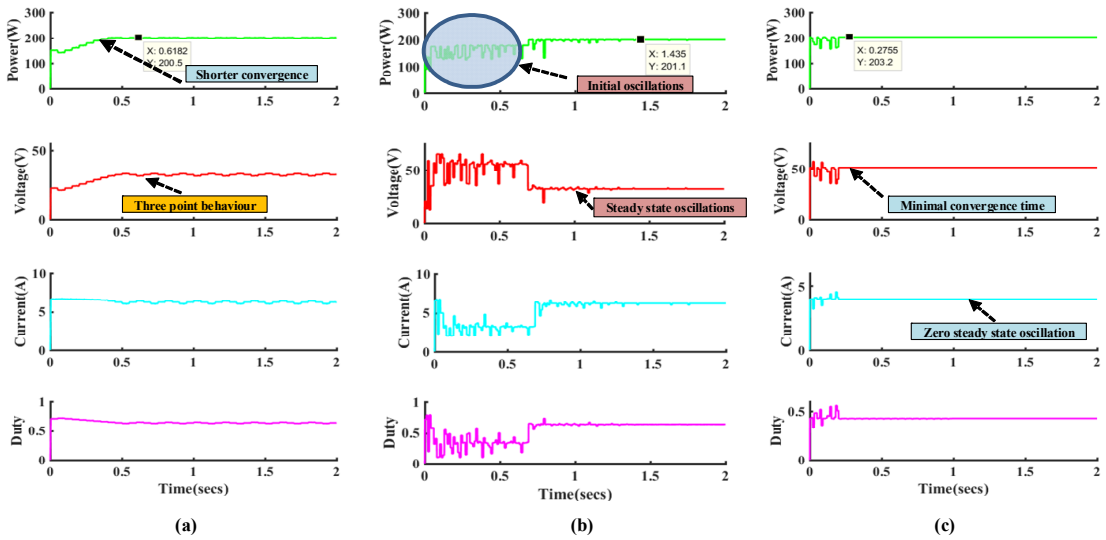

Figure 12. Simulated waveforms of (**a**) P& O, (**b**) PSO, and (**c**) SHO methods for Pattern 3.

4.1.4. Pattern 04 (MPPT under Partial Shading—Four Peaks)

Complexity arises in reaching the global peak when the number of bypasses increases. Hence, to prove the performance of the SHO method under such circumstances, Pattern 4 with three shades causing four peaks is studied. In this case of partial shading, there are four power peaks: the first local peak at 90 W, the second local Peak at 150 W, the third local peak at 140 W, and the global peak at 175 W, respectively. Simulation results of Pattern 4 depicted in Figure 13 illustrate that the P&O method converges to a local peak of 170.9 W. This scenario is expected, since the P&O duty cycle is initialized from the left side of the PV curve. Further, from the simulation results it is understood that both PSO and SHO methods reach a global peak of 210.9 W at 1.5 s and 0.4 s, respectively. However, the PSO method undergoes large transients alongside steady-state oscillations before reaching the global power peak. Moreover, the SHO method consumes only three iterations with zero steady-state oscillations before it reaches global MPP.

Pattern 4

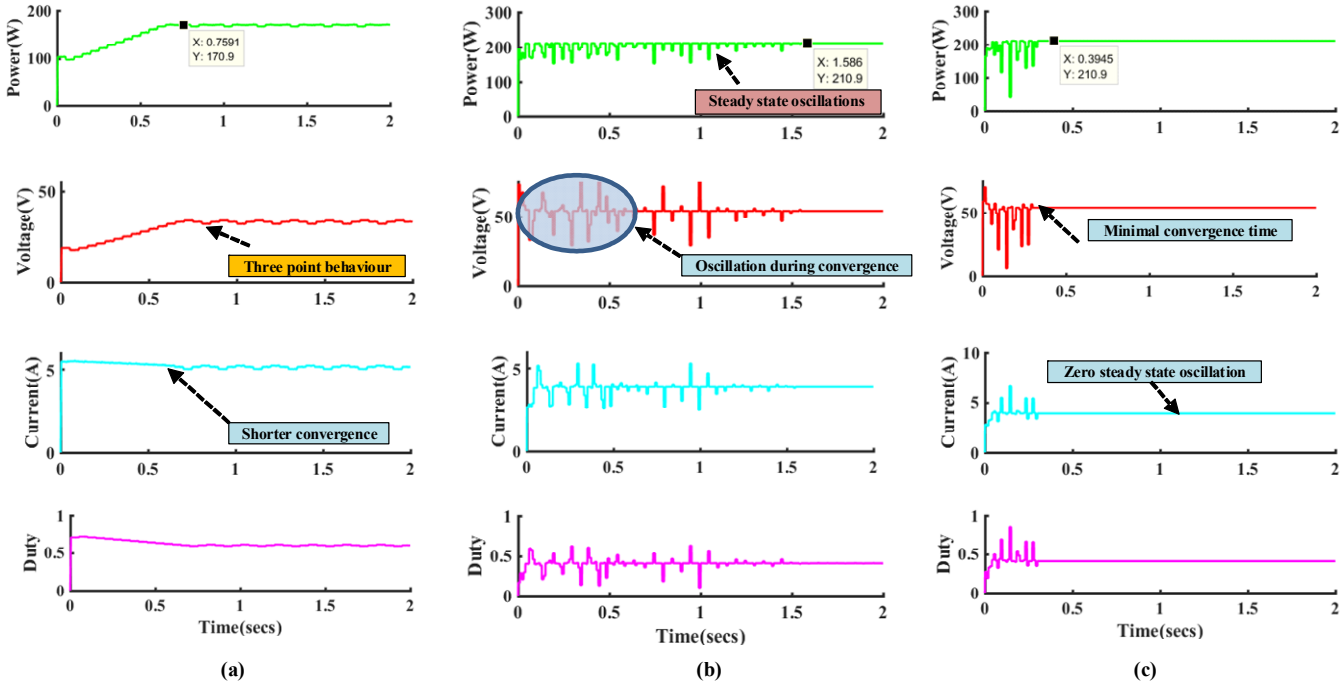

Figure 13. Simulated waveforms of (**a**) P&O, (**b**) PSO, and (**c**) SHO for Pattern 4.

4.1.5. Pattern 05 (5S1P: MPPT under Partial Shading—5 Peaks)

In order to analyze the performance of the SHO method firmly, more panels were added to form a string with different shades creating five peaks with 5S1P PV-string configuration. In this case of partial shading, five power peaks appeared: the first one a local peak at 42 W, the second one a local peak at 80 W, the third one a global peak at 104 W, the fourth one a local peak at 90 W, and the fifth one a local peak at 55 W. Due to initialization from the left of the MPP, the P&O converged to a local peak of 42 W also it took 0.43 s. Further, PSO converged to a global peak of 104 W with an additional 0.8 s. According to the simulation results indicated in Figure 14, the proposed SHO method converged to a global peak of 104 W in 0.25 s. Most importantly, the PSO and SHO methods achieved global peaks with minimal steady-state oscillations.

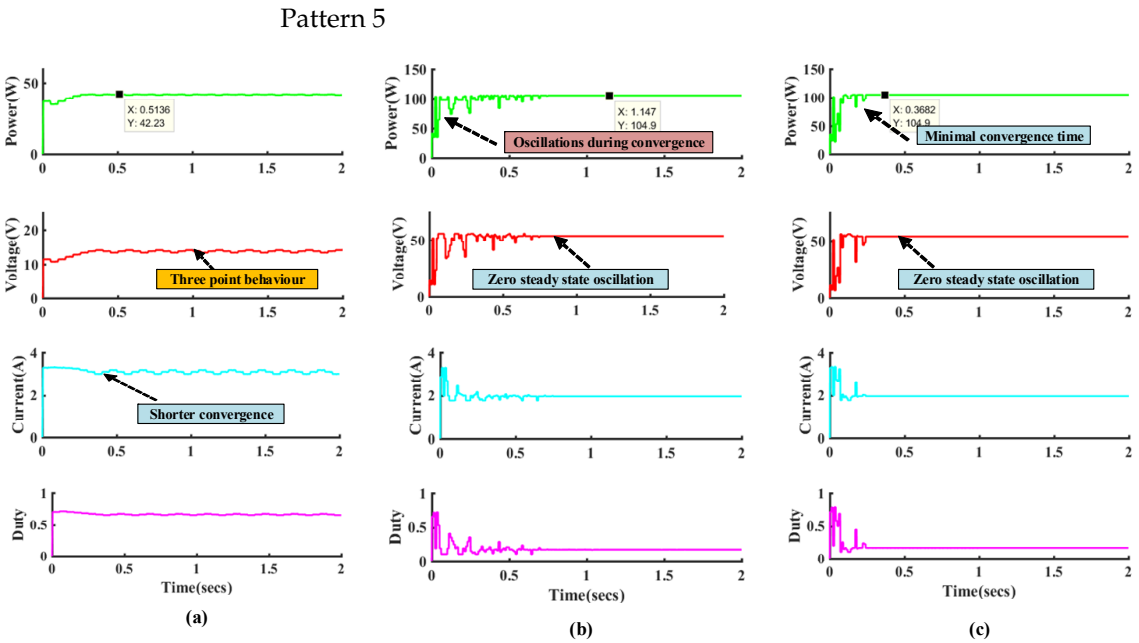

Figure 14. Simulated waveforms of (**a**) P& O, (**b**) PSO, and (**c**) SHO methods for Pattern 5.

4.1.6. Pattern 06 (6S1P: MPPT under Partial Shading—6 Peaks)

Additional performance analysis with more peaks is always helpful in arriving to better conclusions. Therefore, a PV string of size 6S1P with five shades was constructed and tested. In this case of partial shading, six power peaks appear: The first a local peak at 45 W, the second a local peak at 95 W, the third a local peak at 110 W, the fourth a global peak at 118 W, the fifth a local peak at 98 W, and the sixth at 35 W. It is clear to note that the P&O converges to a local peak of 90 W due the initialization from the left to the MPP point, and took 1.44 s. Further, PSO converged to a global peak of 118 W and took 1.1 s. On the other hand, the SHO method converged to global peak of 118 W in 0.27 s. Notably, SHO proved again to be faster than other the two methods, with minimal oscillations, as depicted in Figure 15. Moreover, it is notable that P&O method is not able to converge to a global peak in partial shading when wrongly initiated.

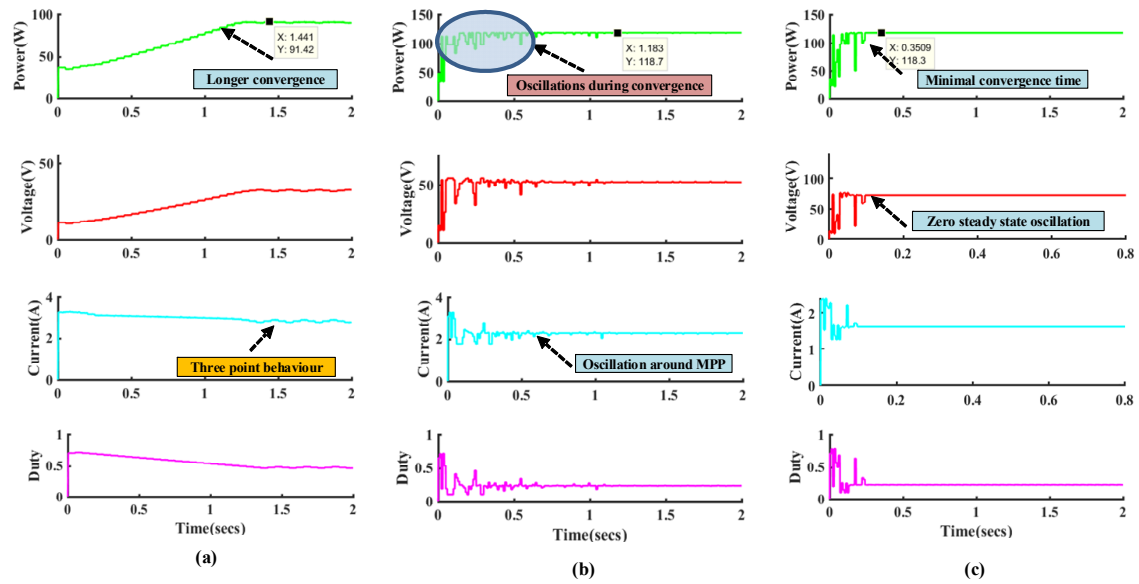

Figure 15. Simulated waveforms of (**a**) P&O, (**b**) PSO, and (**c**) SHO methods for Pattern 6.

4.2. Case Study—B (Step-Change Pattern)

In practical conditions, the PV panel irradiation undergoes changes due to weather conditions, hence it is important to study such transients using step changes in irradiance. In order to identify the occurrence of partial-shading conditions/Irradiation Change (IC), threshold changes in voltage and current values between iterations are noted. When any insolation change occurs, the algorithm is reinitialized and starts its search process. In order to account for any insolation changes, numerous simulations were performed based on a trial-and-error method considering large and small ICs. From the results, the optimum values of 0.1 and 0.2 were obtained for voltage and current, respectively. Moreover, the same values replicated in the literature are an apparent indication of the judicial investigation of the SHO method. Therefore, the occurrence of IC can be detected by the following condition [31].

$$\frac{V_{PV}(k) - V_{PV}(k-1)}{V_{PV}(k)} \geq 0.2 \tag{12}$$

$$\frac{I_{PV}(k) - I_{PV}(k-1)}{I_{PV}(k)} \geq 0.1 \tag{13}$$

where '$V_{PV}(k)$' is the PV voltage at the kth iteration; '$V_{PV}(k-1)$' is the PV voltage in the previous iteration; '$I_{PV}(k)$' is the PV current at the kth iteration; and '$I_{PV}(k-1)$' is the PV current at the previous iteration.

4.2.1. Step Change from Pattern 2 to Pattern 4 for 4S2P

The step change from Patterns 2 to 4 for the 4S2P configuration is depicted in Figure 16. From the simulation result, it is clear that SHO converged to a global peak of 315 W in 0.85 s for Pattern 2 with minimal oscillation. Further, P&O and PSO converged to a global peak of 315 W in 1.3 s and 1.4 s, respectively. However, the P&O oscillation was lower compared to PSO and SHO due the linear change in duty cycle.

Case B: Pattern Change from Pattern 2 to Pattern 4 (4S2P)

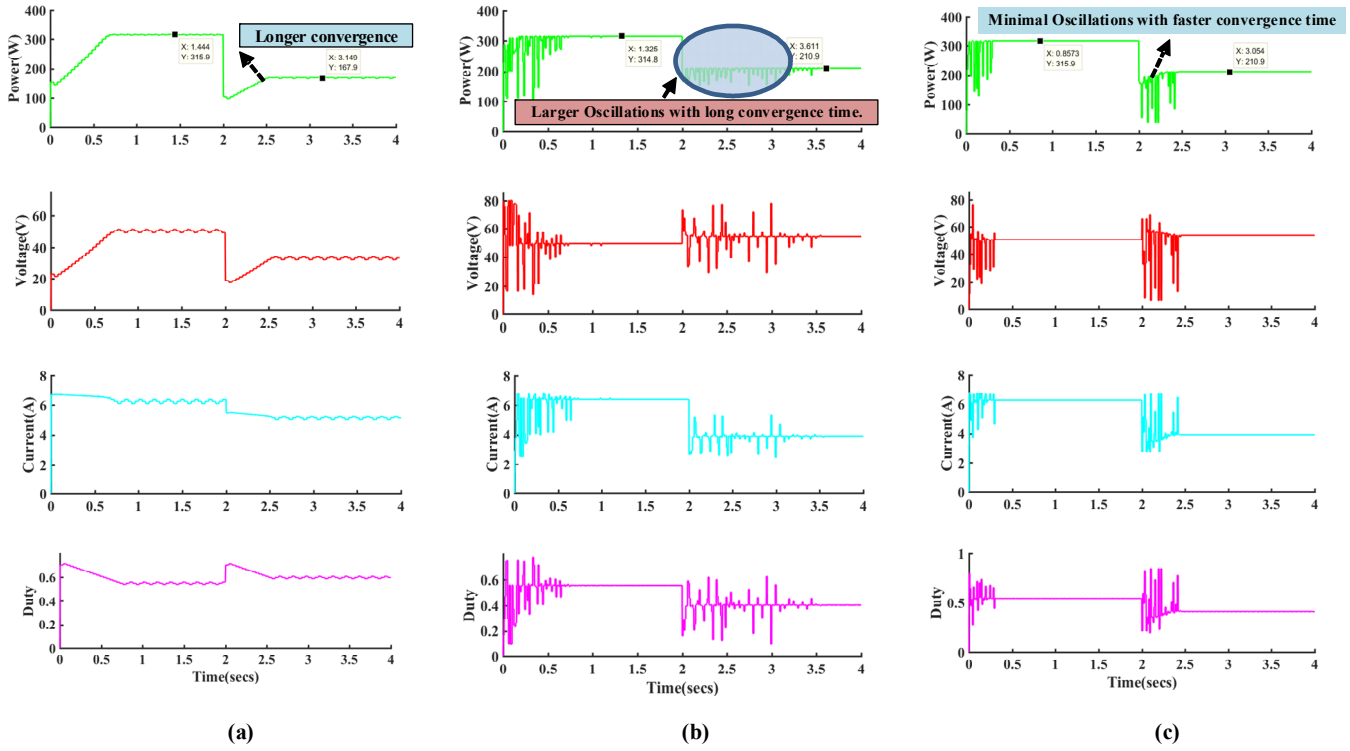

Figure 16. Simulated waveforms of (**a**) P& O, (**b**) PSO, and (**c**) SHO methods for pattern change in 4S2P configuration from Pattern 2 to Pattern 4.

After 2 s, the irradiation pattern change from 2 to 4 was initiated to check the dynamic behavior of the algorithm, and the simulation results are clear that SHO converged to a global peak of 210 W in 0.3 s for pattern 4, whereas PSO converged to the same global peak of 210 W in 1.44 s and P&O converged to a local peak of 168 W in 1.1 s. Notably, P&O did not reached a global peak for Pattern 4 due to the duty cycle initiating from the left part of the curve.

4.2.2. Step Change from Uniform Irradiation to Pattern 5 for 5S1P

It is important to evaluate the step-pattern change from a uniform to higher PV panel configuration to access method efficiency.

Simulated waveforms with uniform irradiation are presented in Figure 17, and it is observed that SHO converged to a global peak of 275 W in 0.94 s for uniform irradiation with minimal oscillation. Further, the P&O and PSO methods converged to a global peak of 275 W in 0.94 s and 1.3 s, respectively. However, the P&O oscillation was lower compared to PSO and SHO due the linear change in duty cycle for P&O.

Pattern Change from Uniform to Pattern 5 (5S1P)

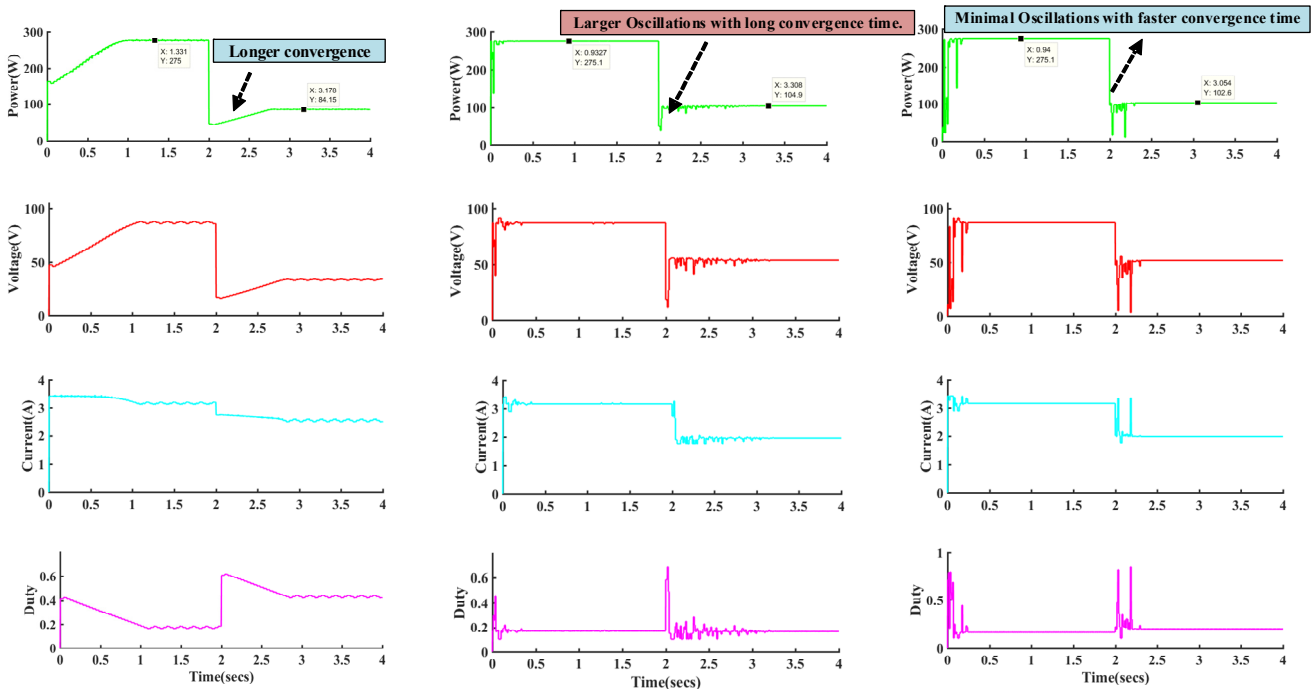

Figure 17. Simulated waveforms of (**a**) P& O, (**b**) PSO, and (**c**) SHO methods for pattern change in 5S1P configuration from uniform irradiation to Pattern 5.

After 2 s of running, the irradiation pattern changed from uniform to Pattern 5 to check the dynamic behavior of algorithm. The simulation result depicted in Figure 18 shows that SHO converged to a global peak of 103 W in 0.25 s for Pattern 5, whereas P&O converged to a local peak of 84 W in 1.2 s and PSO converged to a global peak of 104 W in 1.3 s.

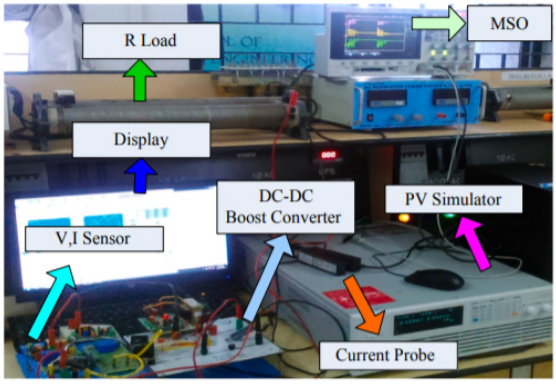

Figure 18. Experimental setup of DC–DC boost converter developed for SHO methods.

Performance summary of all defined pattern results are tabulated in below Table 2.

Table 2. Comparative analysis of P and O, PSO, and SHO methods.

S. No	Configuration	Pattern Number	Method	Maximum Power from PV Curve (Watts)	V_{mpp} (V)	I_{mpp} (A)	P_{mpp} (W)	Efficiency (η)	Tracking Speed (s)
1.	4S2P	1	SHO	439.8	68.6	6.399	439	99.81	0.34
			PSO		68.6	6.399	439	99.81	0.78
			P & O		68.6	6.399	439	99.81	1.35
		2	SHO	320.2	52.18	6.107	318.7	99.53	0.24
			PSO		50.49	6.257	315.9	98.65	1.23
			P & O		50.49	6.257	315	98.37	0.95
		3	SHO	206.8	51.23	3.966	203.2	98.25	0.2
			PSO		32.37	6.21	201.1	97.24	1.4
			P & O		32.32	6.223	201.1	97.24	0.61
		4	SHO	213.1	54.02	3.904	210.9	98.96	0.3
			PSO		54.01	3.904	210.9	98.96	1.5
			P & O		33.15	5.192	172.1	80.76	0.87
2.	5S1P	5	SHO	105	53.81	1.949	104.9	99.90	0.25
			PSO		53.81	1.949	104.9	99.90	0.8
			P & O		13.7	3.083	42.23	40.21	0.43
3.	6S1P	6	SHO	120.2	52.93	2.234	118.3	98.41	0.27
			PSO		52.32	2.268	118.7	98.75	1.1
			P & O		31.94	2.2775	89.88	74.77	1.44

4.3. Results Comparison

The comparison of any optimization method proposed for the application of MPPT depends on the convergence time, sampling time, type of DC–DC converter, switching frequency of the DC–DC converter, operating duty-cycle range, and the number of search agents used. In this article, a boost converter with specifications mentioned in Table 1 is used for both simulations and experimentations with minimum of five search agents. Further, to emphasize the superiority of the SHO algorithm, a comparative table (Tables 3 and 4) based on sampling time (t_s) and convergence time (t_c) is prepared and presented. Here, the SHO algorithm's performance is compared with a recently proposed MCA and improved cuckoo search for one peak and five peak conditions. Furthermore, the two new variants of PSO, i.e., nested PSO and fast adaptive PSO, are also compared in Table 4. However, the defined search agents, converter-switching frequency, and sample time of the above-

mentioned methods differ. SHO executes much better compared to the MCA, ICS, and nested PSO methods, with a faster settling time and fewer oscillations under uniform and partial-shading conditions (one and five peaks). Moreover, it also outperforms the nested PSO and FA-PSO for three peaks in the MPP curve.

Table 3. Comparative results of SHO, MCA, and improved cuckoo search algorithms for one and five Peaks.

Methods	One Peak		Five Peaks	
	t_c	t_s	t_c	t_s
SHO	0.34	0.02	0.25	0.02
MCA [23]	0.354	0.01	0.36	0.01
ICS [20]	0.4	0.01	0.25	0.01
Nested PSO [29]	1.515	0.05	2.04	0.05

Table 4. Comparative results of SHO, nested PSO, and FA-PSO algorithms for three peaks.

Methods	Three Peaks	
	t_c	t_s
SHO	0.34	0.02
Nested PSO [29]	1.85	0.05
FA-PSO [30]	0.4	0.1

4.4. Hardware Implementation

4.4.1. Pattern 01 (MPPT under Zero or Uniform Shading)

The experimental results of Pattern 01, i.e., the 4S2P PV-array system under zero or uniform shade conditions are plotted in Figure 19. The convergence of P&O falls in line with the simulation results in terms of three-point behavior. Among the three methods, P&O takes a longer time to settle, i.e., 1.32 s to reach global peak. Following the P&O method, PSO takes 0.75 s. Above all, SHO takes the lowest convergence time of 0.4 s among the methods. Moreover, SHO's performance is superior only in terms of time taken at uniform shading, as the remaining methods also reach a global peak.

4.4.2. Hardware Experimental Result: Pattern 03 (MPPT under Partial Shading—3 Peaks)

In Pattern 03, a solar-array simulator generates three power peaks to know the capability of the SHO method and its ability to differentiate between the global and local peak. It is evident from results that all three methods reach a global peak of 250 W; surprisingly, P&O reaches this peak value in a shorter time of 0.6 s compared to the PSO method, while the P&O method takes 1.4 s, the longest among all the methods. From the experimental results plotted in Figure 20, SHO takes the shortest time interval to global peak convergence. The performance of SHO is proved to be superior at partial shading, with three peaks in comparison with P&O and PSO.

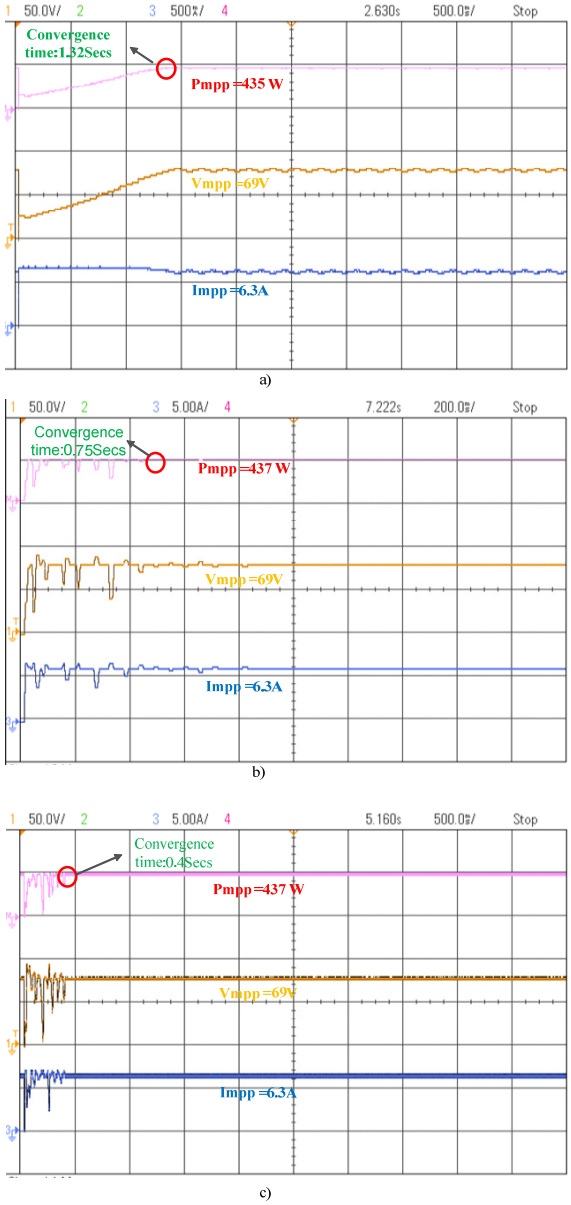

Figure 19. Experimental result for Pattern 1 under uniform shading (**a**) P&O, (**b**) PSO, (**c**) SHO.

4.4.3. Hardware Experimental Result: Pattern 05 (5S1P: MPPT under Partial Shading—5 Peaks)

In order to firmly measure SHO performance, panels of 5S1P PV-string configuration were subjected to additional shades, creating five peaks for experimentation, and results were recorded. Due to initialization from the left of the MPP, P&O converges to a local peak (not reaching global peak) of 42.0 W. However, PSO and SHO are able to converge to a global peak 105.0 W. The experimental results are indicated in Figure 21. The performance of SHO is proved to be superior at partial shading, with five peaks in comparison with the P&O and PSO techniques. The simulation results and experimental results are matching, with minor variations.

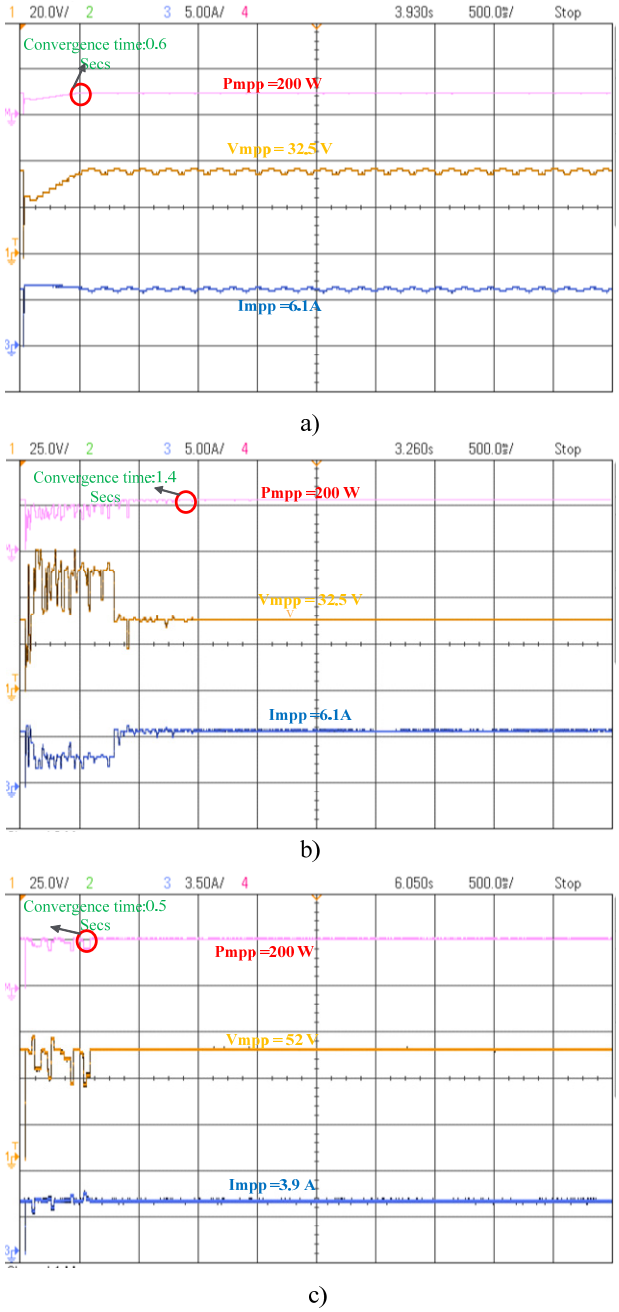

Figure 20. Experimental result for Pattern 3 under partial shading (**a**) P&O, (**b**) PSO, (**c**) SHO.

4.4.4. Hardware Experimental Result: Pattern 06 (6S1P: MPPT under Partial Shading—6 Peaks)

The firm and accurate performance of SHO was experimented, with more panels n the string applied with different shades, creating six peaks for 6S1P PV-string configuration, and results are tabulated. Due to initialization from the left of the MPP, P&O converged to a local peak (not reaching a global peak) of 90.0 W. However, PSO and SHO were able to converge to a global peak 120.0 W. The experimental results are indicated in Figure 22. The performance of SHO is proved to be superior at partial shading, with six peaks in comparison to the P&O and PSO techniques.

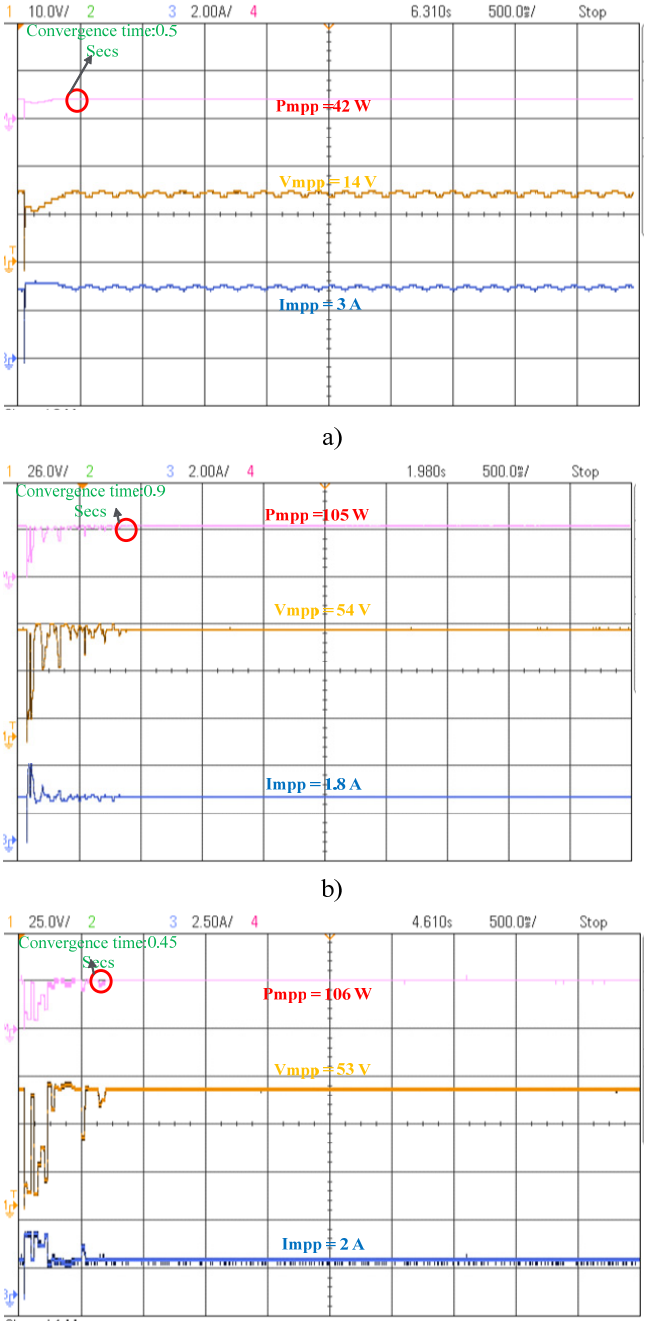

Figure 21. Experimental result for Pattern 5 under partial shading (**a**) P&O, (**b**) PSO, (**c**) SHO.

4.5. Case Study B (Step-Change Pattern)

Two additional cases with step-change behavior were analyzed from the viewpoint of the practical condition of sudden changes in weather conditions. The step change was applied for 4S2P and 5S1P PV array.

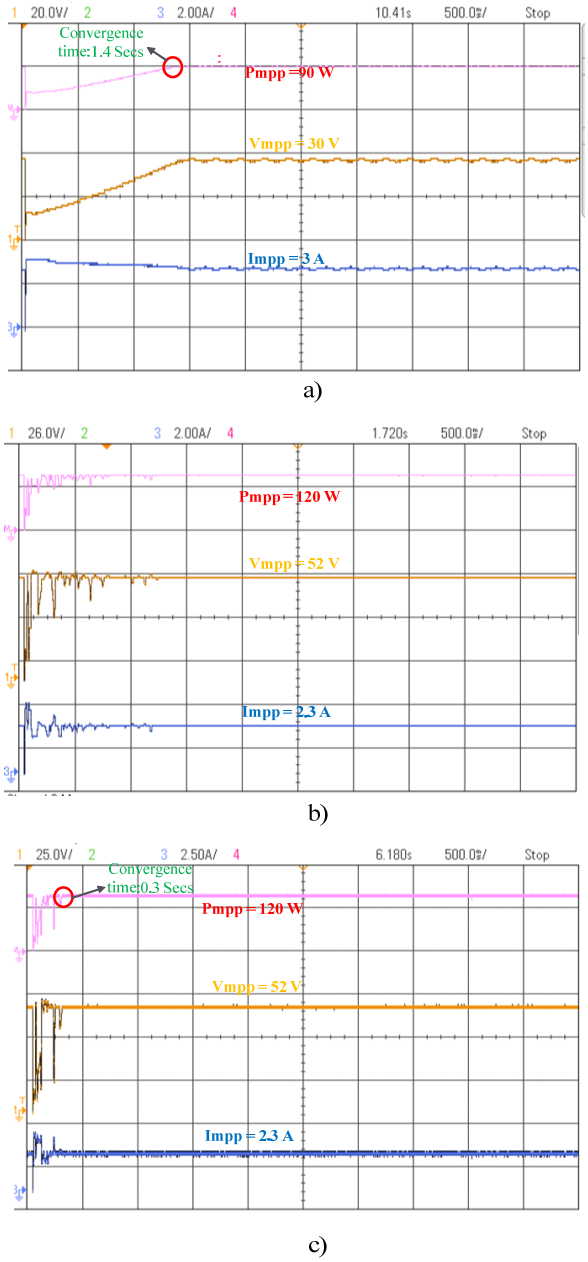

Figure 22. Experimental result for Pattern 6 under partial shading (**a**) P&O, (**b**) PSO, (**c**) SHO.

4.5.1. Step Change from Pattern 2 to Pattern 4 for 4S2P

The experimental result for the step change from Patterns 2 to 4 for 4S2P configuration is presented in Figure 23. From the experimental result it is clear that SHO converged fast to a global peak of 315.0 W in 0.3 s for Pattern 2, with minimal oscillation compared to P&O and PSO. The step change was then initiated after 2 s. A few observations can be made from the experimental results: (1) Step change forces the algorithm to search for a new global peak under PS; (2) a new search for a global peak helps in the behavior characterization of the method under transient changes. The experimental results indicate that as the number of peaks increases in both the cases; (3) the PSO method produces high oscillation in both patterns with the longest time for convergence. Comparatively, P&O takes a shorter time interval even though it reaches a local peak in one of the patterns. Meanwhile, SHO proved to be superior in performance both in terms of time taken and convergence to a global peak with lower oscillation. This behavior matches well with the simulation case.

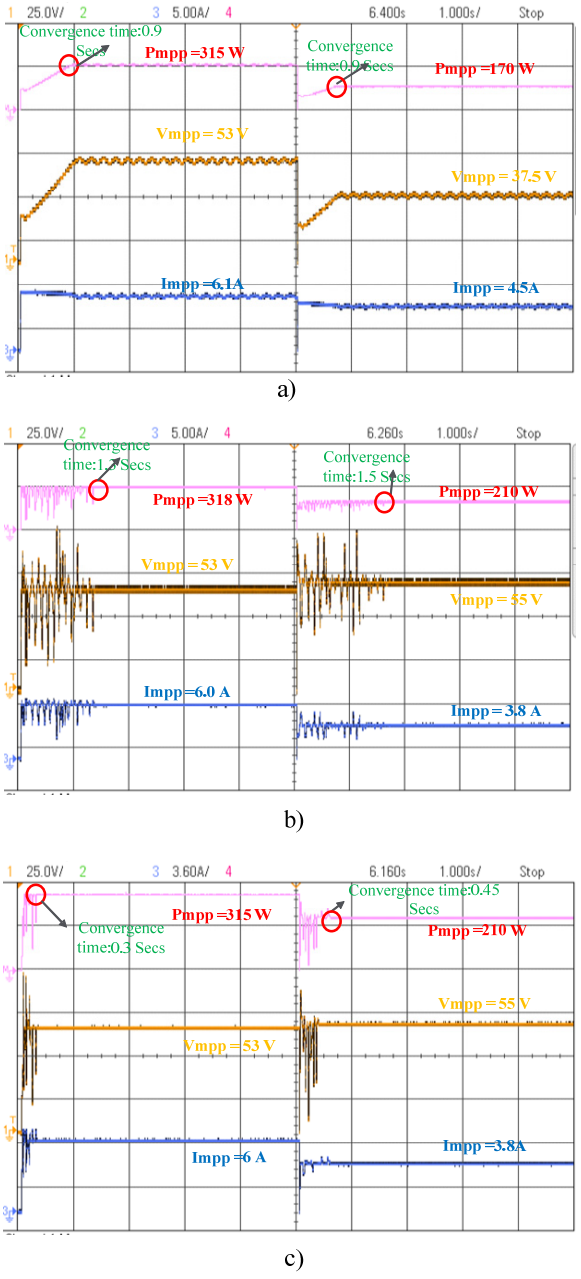

Figure 23. Experimental result for Pattern change from 2 to 4 under partial shading: (**a**) P&O, (**b**) PSO, (**c**) SHO.

4.5.2. Step Change from Uniform Irradiation to Pattern 5 for 5S1P

Figure 24 describes the experimental results for the step change from uniform irradiation to Pattern 5 for 5S1P configuration. The experimental results show that SHO converged quickly to a global peak of 270.0 W in 0.5 s for the uniform pattern with minimal oscillation compared to P&O and PSO. After 2 s of running, the irradiation pattern changed from uniform to 5 and SHO converged quickly to a global peak of 106.0 W in 0.45 s for Pattern 5 compared to PSO and P&O. The simulation results and experimental results are matching, with minor variations.

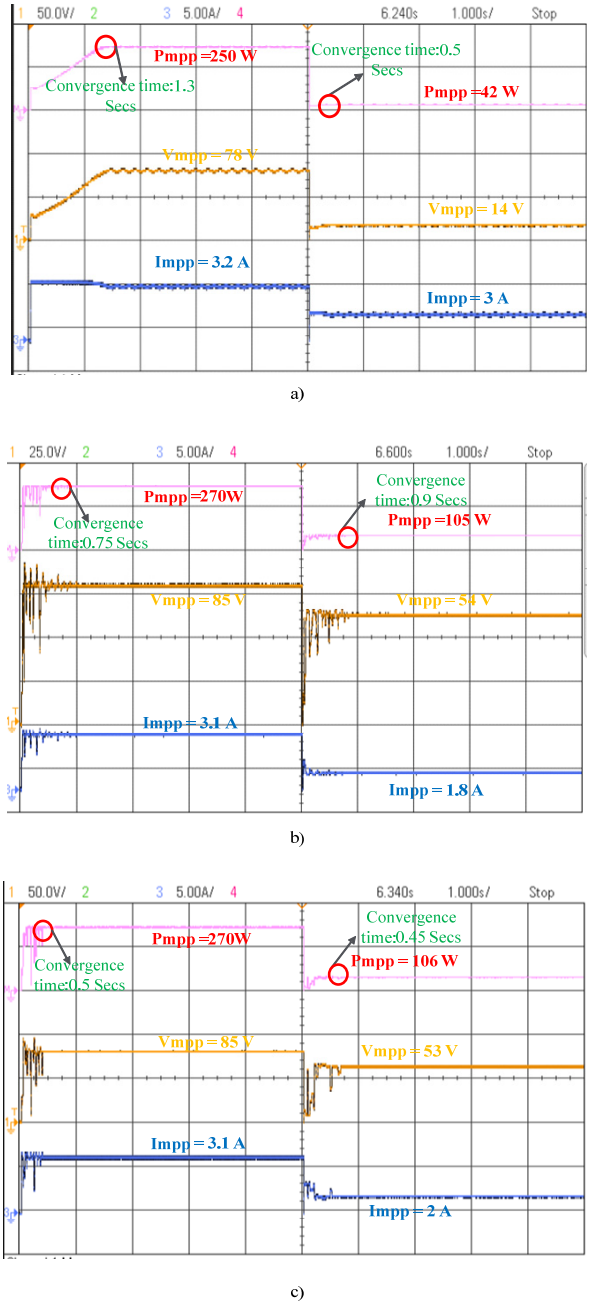

Figure 24. Experimental result for Pattern change from uniform shading to partial of Pattern 5: (**a**) P&O, (**b**) PSO, (**c**) SHO.

5. Analysis on Energy Saving

The efficient use of energy boosts a country's income-generating activities and enhances its overall economic status. In addition to the software simulation and hardware results analysis, a few parameters such as energy saving, units produced, and income generated are analyzed. Though the previous discussions indicate the supremacy of the SHO method in terms of convergence to global maxima and time taken for convergence, it is advisable to evaluate the economic impact as well as its practical significance. Therefore, energy-saving analysis for real-time conditions is carried out. For experimentation, the hardware setup was arranged at the Technology Tower building of VIT University, Vellore was utilized. For this analysis, an average sunshine time of 5 h/day was considered and different patterns were applied between 10:00 a.m.–3:00 p.m. The solar rooftop PV-plant capacity installed at VIT was 1 kW. For practical significance, five patterns (Patter 1–5) with

different shade intensities were applied at an interval of 1 h. All the algorithm performances were monitored for a period of 5 h a day and presented in Table 5. From the below Table 5, it can be observed that SHO produces the highest number of units generated per day compared to PSO and P&O. The impact on energy generated by SHO is also noticeable.

Table 5. Economical Assessment of different methods.

Pattern	Energy Generated in Whr			Unit Generated		
	SHO	**PSO**	**P&O**	**SHO**	**PSO**	**P&O**
Pattern 01 for 10:00–11.00 a.m.	439	439	439	0.439	0.439	0.439
Pattern 02 for 11:00–12:00 noon	320	315	315	0.32	0.315	0.315
Pattern 03 for 12:00–1:00 p.m.	203	201	201	0.203	0.201	0.201
Pattern 04 for 1:00–2:00 p.m.	211	211	172	0.211	0.211	0.172
Pattern 05 for 2:00–3:00 p.m.	105	105	42	0.105	0.105	0.042
Net Energy Generated/Day	1278	1271	1169	1.278	1.271	1.169
Net Energy Generated/Year (280 days considered)	357,840	355,880	327,320	357.84	355.88	327.32
Total Income Generated @ INR 10 per Unit				3578	3559	3273.2

The revenue generated by SHO is comparatively higher than PSO and P&O. Although the income generated between SHO and PSO has a minor difference, it will have significant impact for the larger solar power-plant application.

6. Conclusions

In this work, the Spotted Hyena Optimizer (SHO) algorithm for global MPP tracking is proposed and validated for several partial-shading scenarios. The proposed technique for all shade patterns tracked the highest power at a shorter tracking time compared to PSO and P&O. The comparative results are extremely satisfying and also deliver an in-depth elucidation about the supremacy of the proposed method in tracking the global peak. For all the shade patterns considered, the SHO method outperformed all the methods considered. For instance:

1. In the case of shade Pattern 01, even though SHO, PSO, and P&O were able to track global peak, the convergence times of SHO were 4 and 2 times shorter than P&O and PSO.
2. For Pattern 2, SHO generated 2% higher power compared to P&O and better convergence time compared to PSO and P&O.
3. Similarly for shade Patterns 3 and 4, the convergence times of SHO were 3 and 7 times shorter than P&O and PSO.
4. Even for shade Patterns 5 and 6, the proposed technique retained its first position in attaining better convergence at a shorter time.

The outcomes of the simulation and hardware results have strengthened the belief that SHO is effective in tracking optimal power in less time. Hence, the proposed technique is suitable and highly recommended to track the maximum power point effectively for complex PSCs.

Author Contributions: Conceptualization, E.R. and R.N.; methodology, E.R. and R.N.; software, E.R.; validation, E.R. and R.N.; formal analysis, E.R.; investigation, E.R. and R.N.; resources, E.R.; data curation, E.R.; writing—original draft preparation, E.R. and R.N.; writing—review and editing, E.R. and R.N.; visualization, E.R. and R.N.; supervision, R.N. All authors have read and agreed to the published version of the manuscript.

Funding: This research received no external funding.

Informed Consent Statement: Not applicable.

Data Availability Statement: Not applicable.

Acknowledgments: This work was carried out at Solar Energy Research Cell (SERC), School Electrical Engineering (SELECT), Vellore Institute of Technology (VIT), Vellore. Hereby, the authors would like to thank VIT management for their support in providing the lab facility to carry out this work.

Conflicts of Interest: The authors declare no conflict of interest.

Nomenclature

STC	Standard Test Conditions
PV	Photovoltaic
TCT	Total Cross Tied
PS	Partial Shading
MPPT	Maximum Power Point Tracking
IPV & VPV	Current and voltage generated by a PV cell
IO &VO	Output current and voltage of a PV module
ID	Diode current
Ish & Iph	Shunt current and Photo-generated current
Rs, Rp	Series and Shunt resistances
G& GSTC	Irradiance (W/m^2) and Irradiance level at standard testing conditions
ANN	Artificial Neural Network
SSO	Salp-Swarm Optimization
MFO	Moth-Flame optimization
HC	Hill Climbing
Inc. Cond.	Incremental Conductance
FLC	Fuzzy Logic Control
GWO	Grey-Wolf Optimization
WDO	Wind-Driven Optimization
SHO	Spotted-Hyena Optimizer
P&O	Perturb and Observe

References

1. Solar Industry Growing at a Record Pace. Available online: https://www.seia.org/solar-industry-research-data (accessed on 12 February 2022).
2. Ram, J.P.; Babu, T.S.; Rajasekar, N. A comprehensive review on solar PV maximum power point tracking techniques. *Renew. Sustain. Energy Rev.* **2017**, *67*, 826–847. [CrossRef]
3. Eltawil, M.A.; Zhao, Z. MPPT techniques for photovoltaic applications. *Renew. Sustain. Energy Rev.* **2013**, *25*, 793–813. [CrossRef]
4. Al Mamun, M.A.; Hasanuzzaman, M.; Selvaraj, J. Experimental investigation of the effect of partial shading on photovoltaic performance. *IET Renew. Power Gener.* **2017**, *11*, 912–921. [CrossRef]
5. Mutoh, N.; Matuo, T.; Okada, K.; Sakai, M. Prediction-data-based maximum-power-point-tracking method for photovoltaic power generation systems. In Proceedings of the 2002 IEEE 33rd Annual IEEE Power Electronics Specialists Conference, Cairns, QLD, Australia, 23–27 June 2002; Volume 3, pp. 1489–1494.
6. Wolfs, P.J.; Tang, L. A single cell maximum power point tracking converter without a current sensor for high performance vehicle solar arrays. In Proceedings of the 2005 IEEE 36th Power Electronics Specialists Conference, Recife, Brazil, 12–16 June 2005; Volume 2005, pp. 165–171.
7. Safari, A.; Mekhilef, S. Simulation and hardware implementation of incremental conductance MPPT with direct control method using cuk converter. *IEEE Trans. Ind. Electron.* **2011**, *58*, 1154–1161. [CrossRef]
8. De Brito, M.A.G.; Galotto, L.; Sampaio, L.P.; Melo, G.D.; Canesin, C.A. Evaluation of the main MPPT techniques for photovoltaic applications. *IEEE Trans. Ind. Electron.* **2013**, *60*, 1156–1167. [CrossRef]
9. Ahmad, J. A fractional open circuit voltage based maximum power point tracker for photovoltaic arrays. In Proceedings of the IEEE 2010 2nd International Conference on Software Technology and Engineering, San Juan, PR, USA, 25 October 2010; Volume 1.
10. Alajmi, B.N.; Ahmed, K.H.; Finney, S.J.; Williams, B.W. Fuzzy-logic-control approach of a modified hill-climbing method for maximum power point in microgrid standalone photovoltaic system. *IEEE Trans. Power Electron.* **2011**, *26*, 1022–1030. [CrossRef]
11. Rai, A.K.; Kaushika, N.D.; Singh, B.; Agarwal, N. Simulation model of ANN based maximum power point tracking controller for solar PV system. *Sol. Energy Mater. Sol. Cells* **2011**, *95*, 773–778. [CrossRef]
12. Ram, J.P.; Rajasekar, N. A Novel Flower Pollination Based Global Maximum Power Point Method for Solar Maximum Power Point Tracking. *IEEE Trans. Power Electron.* **2017**, *32*, 8486–8499.

13. Rezk, H.; Fathy, A. Simulation of global MPPT based on teaching–learning-based optimization technique for partially shaded PV system. *Electr. Eng.* **2017**, *99*, 847–859. [CrossRef]
14. Sangeetha, K.; Babu, T.S.; Rajasekar, N. Fireworks Algorithm-Based Maximum Power Point Tracking for Uniform Irradiation as Well as Under Partial Shading Condition. In *Artificial Intelligence and Evolutionary Computations in Engineering Systems*; Springer: New Delhi, India, 2016; pp. 79–88.
15. Abdalla, O.; Rezk, H.; Ahmed, E.M. Wind driven optimization algorithm based global MPPT for PV system under non-uniform solar irradiance. *Sol. Energy* **2019**, *180*, 429–444. [CrossRef]
16. Mirza, A.F.; Mansoor, M.; Ling, Q.; Yin, B.; Javed, M.Y. A Salp-Swarm Optimization based MPPT technique for harvesting maximum energy from PV systems under partial shading conditions. *Energy Convers. Manag.* **2020**, *209*, 112625. [CrossRef]
17. Shi, J.Y.; Zhang, D.Y.; Xue, F.; Li, Y.J.; Qiao, W.; Yang, W.J.; Xu, Y.M.; Yang, T. Moth-flame optimization-based maximum power point tracking for photovoltaic systems under partial shading conditions. *J. Power Electron.* **2019**, *19*, 1248–1258.
18. Mohanty, S.; Subudhi, B.; Ray, P.K. A new MPPT design using grey Wolf optimization technique for photovoltaic system under partial shading conditions. *IEEE Trans. Sustain. Energy* **2016**, *7*, 181–188. [CrossRef]
19. Kumar, Y.S.; Gupta, R. Maximum power point tracking of multiple photovoltaic arrays. In Proceedings of the 2012 Students Conference on Engineering and Systems, Allahabad, India, 16–18 March 2012; Volume 47, pp. 367–380.
20. Vysakh, M.; Azharuddin, M.; Vilas, H.; Muralidhar, K.; Paul, D.; Jacob, B.; Rajasekar, N. Maximum power point tracking using modified PSO with CUK Converter. In Proceedings of the 2014 International Conference on Advances in Electrical Engineering (ICAEE), Vellore, India, 9–11 January 2014; Volume 2014.
21. Babu, T.S.; Rajasekar, N.; Sangeetha, K. Modified Particle Swarm Optimization technique based Maximum Power Point Tracking for uniform and under partial shading condition. *Appl. Soft Comput. J.* **2015**, *34*, 613–624. [CrossRef]
22. Sen, T.; Pragallapati, N.; Agarwal, V.; Kumar, R. Global maximum power point tracking of PV arrays under partial shading conditions using a modified particle velocity-based PSO technique. *IET Renew. Power Gener.* **2018**, *12*, 555–564. [CrossRef]
23. Motamarri, R.; Nagu, B. GMPPT by using PSO based on Lévy flight for photovoltaic system under partial shading conditions. *IET Renew. Power Gener.* **2020**, *14*, 1143–1155. [CrossRef]
24. Manickam, C.; Raman, G.R.; Raman, G.P.; Ganesan, S.I.; Nagamani, C. A Hybrid Algorithm for Tracking of GMPP Based on P&O and PSO with Reduced Power Oscillation in String Inverters. *IEEE Trans. Ind. Electron.* **2016**, *63*, 6097–6106.
25. Mao, M.; Zhang, L.; Duan, P.; Duan, Q.; Yang, M. Grid-connected modular PV-Converter system with shuffled frog leaping algorithm based DMPPT controller. *Energy* **2018**, *143*, 181–190. [CrossRef]
26. Eltamaly, A.M.; Farh, H.M.H. Dynamic global maximum power point tracking of the PV systems under variant partial shading using hybrid GWO-FLC. *Sol. Energy* **2019**, *177*, 306–316. [CrossRef]
27. Manickam, C.; Raman, G.P.; Raman, G.R.; Ganesan, S.I.; Chilakapati, N. Fireworks enriched P&O algorithm for GMPPT and detection of partial shading in PV systems. *IEEE Trans. Power Electron.* **2017**, *32*, 4432–4443.
28. Vimalarani, C.; Kamaraj, N. Improved method of maximum power point tracking of photovoltaic (PV) array using hybrid intelligent controller. *Optik* **2018**, *168*, 403–415.
29. Huang, C.; Wang, L.; Long, H.; Luo, X.; Wang, J.H. A hybrid global maximum power point tracking method for photovoltaic arrays under partial shading conditions. *Optik* **2019**, *180*, 665–674. [CrossRef]
30. Ram, J.P.; Pillai, D.S.; Ghias, A.M.Y.M.; Rajasekar, N. Performance enhancement of solar PV systems applying P&O assisted Flower Pollination Algorithm (FPA). *Sol. Energy* **2020**, *199*, 214–229.
31. Dhiman, G.; Kumar, V. Spotted hyena optimizer: A novel bio-inspired based metaheuristic technique for engineering applications. *Adv. Eng. Softw.* **2017**, *114*, 48–70. [CrossRef]
32. Dhiman, G.; Kumar, V. Spotted Hyena Optimizer for Solving Complex and Non-linear Constrained Engineering Problems. In *Harmony Search and Nature Inspired Optimization Algorithms*; Springer: Singapore, 2019; pp. 857–867.
33. Rajasekar, N.; Kumar, N.K.; Venugopalan, R. Bacterial Foraging Algorithm based solar PV parameter estimation. *Sol. Energy* **2013**, *97*, 255–265. [CrossRef]
34. Ram, J.P.; Babu, T.S.; Dragicevic, T.; Rajasekar, N. A new hybrid bee pollinator flower pollination algorithm for solar PV parameter estimation. *Energy Convers. Manag.* **2017**, *135*, 463–476. [CrossRef]
35. Hu, J.; Dong, M.; Shehu, M.M. An ANN-INC MPPT Strategy for Photovoltaic System. In Proceedings of the 2021 IEEE 4th International Electrical and Energy Conference (CIEEC), Nanjing, China, 27–29 May 2022.
36. Motahhir, S.; El Hammoumi, A.; El Ghzizal, A. The most used MPPT algorithms: Review and the suitable low-cost embedded board for each algorithm. *J. Clean. Prod.* **2020**, *246*, 118983. [CrossRef]